

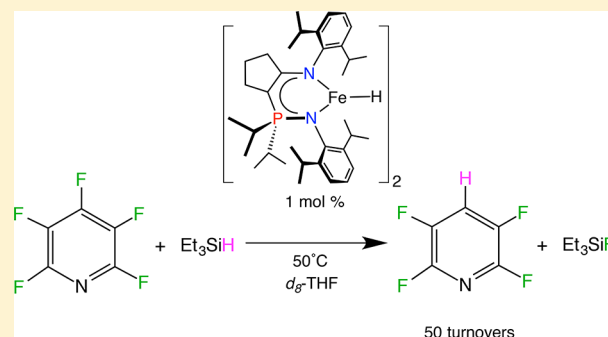
Synthesis and Reactivity of a Low-Coordinate Iron(II) Hydride Complex: Applications in Catalytic Hydrodefluorination

Nicholas M. Hein, Fraser S. Pick, and Michael D. Fryzuk*[✉]

Department of Chemistry, The University of British Columbia, 2036 Main Mall, Vancouver, British Columbia V6T 1Z1, Canada

Supporting Information

ABSTRACT: A low-coordinate iron hydride complex bearing an unsymmetrical NpN (enamido–phosphinimine) ligand scaffold was synthesized and fully characterized. Insertion reactivity with azobenzene, 3-hexyne, and 1-azidoadamantane was explored, and the isolated products were analogous to previously reported β -diketiminato iron hydride insertion products. Surprisingly, the NpN iron hydride displays unprecedented reactivity toward hexafluorobenzene, affording an NpN iron fluoride complex and pentafluorobenzene as products. The NpN iron hydride is a pre-catalyst for catalytic hydro-defluorination of perfluorinated aromatics in the presence of silane. Kinetic studies indicated that the rate-determining step during catalysis involved silane.



INTRODUCTION

The reactivity patterns of low-coordinate first-row transition-metal complexes are well-documented with regard to small-molecule activation and catalytic processes.^{1–6} Of particular interest is the family of variously substituted β -diketiminato (Nacnac) iron hydrides, for example, [(Nacnac)Fe]₂(μ -H)₂,^{7,8} which are highly reactive species. These complexes undergo insertion processes, such as hydride insertion into the N–N double bond of azobenzene,⁹ the C–C triple bond of alkynes,^{8,9} and across the azido group of 1-azidoadamantane.⁸ However, the utilization of low-coordinate iron hydride species as catalyst precursors has been limited. It has been noted that the Fe–H bond in low-coordinate species is unstable, leading to insertion reactions favoring the formation of stronger Fe–X bonds (X = C, N, O).^{10,11} Considering the enthalpic driving force for the breakage of Fe–H and the consequent formation of stronger Fe–X bonds, a natural extension of this reactivity would be the use of iron hydrides to cleave strong C–F bonds, resulting in the subsequent formation of Fe–F bonds. Fluorinated organics have become ubiquitous in the pharmaceutical and agrochemical industry due to their useful chemical properties and stability.^{12,13} However, it is this stability that also presents an environmental challenge, as these organofluorine molecules are often persistent in the biosphere.¹⁴ Thus, removing fluorine atoms via catalytic hydro-defluorination (HDF) for remediation purposes is an important area of research.

The use of late transition-metal complexes for homogeneous HDF catalysis has been an active area of research since the initial report of hexafluorobenzene HDF by a Rh(I)-silyl complex.¹⁵ Since this discovery, there have been numerous examples of catalysts that utilize Ni,^{16,17} Au,^{18,19} Ir,²⁰ and Ru^{21,22} for the HDF of perfluorinated aromatics. For example, the HDF of pentafluoronitrobenzene with a Xantphos-stabilized Au(I)

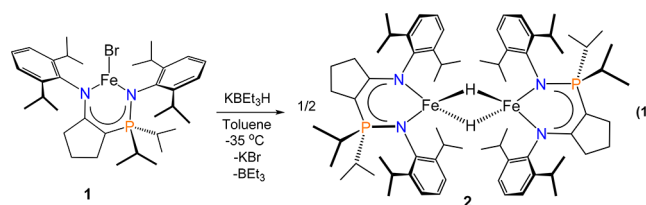
species is highly active and is reported to have a turnover number (TON) of 1000.¹⁹ However, use of the earth-abundant metal Fe for catalytic HDF is limited to one example in the literature,²³ making the further expansion of Fe-based HDF systems a point of interest.

This paper describes the synthesis and characterization of a low-coordinate, paramagnetic iron hydride complex bearing an electronically unsymmetric enamido–phosphinimine (NpN) ligand scaffold. Given the use of Nacnac–iron fluoride complexes in concert with Et₃SiH for the hydro-defluorination of certain fluorinated aromatics,²³ we were interested in examining our NpN donor set in combination with iron in HDF to ascertain the effect of this Nacnac mimic ligand scaffold on this important process.

RESULTS AND DISCUSSION

Synthesis of Low-Coordinate Iron(II) Hydrides.

We previously reported the synthesis and reduction chemistry of the three-coordinate iron(II) bromide complex ((^{CY5}NpN)^{DIPP,DIPP})-FeBr, **1**.²⁴ Treatment of **1** with potassium triethylborohydride serves as a convenient route for the synthesis of the desired low-coordinate iron hydride complexes [(^{CY5}NpN)^{DIPP,DIPP}]-FeH]₂ **2** (eq 1).



Received: August 31, 2017

Single crystals of **2** were grown from a toluene solution of the product cooled to $-35\text{ }^{\circ}\text{C}$. The solid-state structure for **2** is shown below in Figure 1. The bridging hydrides in **2** were

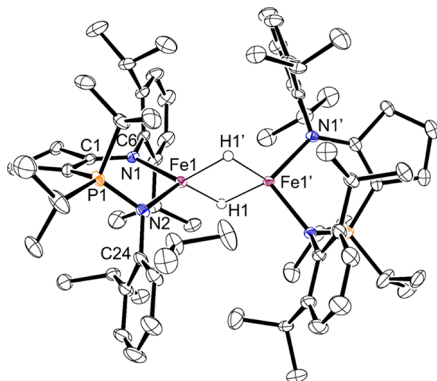


Figure 1. ORTEP drawing of the solid-state molecular structure of **2** (ellipsoids at 50% probability level). All hydrogen atoms except those bonded to iron were omitted for clarity. Selected bond lengths (Å), angles (deg), and torsion angles (deg): Fe1–H1:1.713(19), Fe1–H1':1.789(17), Fe1–Fe1': 2.6762(4), N1–Fe1:2.0461(9), N2–Fe1:2.0455(9), H1–Fe1–H1': 48.4(7), N1–Fe1–N2:99.60(4), C1–N1–C6:115.66(9), P1–N2–C24:119.63(8), N1–Fe1–Fe1'–N1': 37.17(8).

located in the difference density map and were freely refined without constraining the Fe–H bond distance. In comparison to the most closely related Nacnac complex $[(^{\text{tBu}}\text{Nacnac}^{\text{DIPP}})\text{FeH}]_2$, the distance between the two iron centers in **2** is longer (2.6762(4) Å) in contrast to the distance of 2.624(2) Å for the aforementioned Nacnac iron derivative.⁹ This is a surprising result, as the aryl rings in $[(^{\text{tBu}}\text{Nacnac}^{\text{DIPP}})\text{FeH}]_2$ experience more steric clash with the *tert*-butyl groups in the backbone of Nacnac in comparison to the sterics present in the ligand backbone of **2**. This effect is quantified by the C–N–C angle, where the aryl rings present on the N-donors are forced toward the Fe center, which for $[(^{\text{tBu}}\text{Nacnac}^{\text{DIPP}})\text{FeH}]_2$ has an average

value of $121.3(6)^{\circ}$.⁹ The two corresponding angles for **2** are C1–N1–C6:115.66(9) and P1–N2–C24:119.63(8). On the basis of this analysis of ligand sterics, it can be rationalized that the elongated distance between the iron centers in **2** in comparison to $[(^{\text{tBu}}\text{Nacnac}^{\text{DIPP}})\text{FeH}]_2$ is likely electronic in nature.

The ^1H NMR spectra of **2** in d_6 -benzene and d_8 -THF (THF = tetrahydrofuran) are virtually identical at $25\text{ }^{\circ}\text{C}$ (Figure 2) indicating that the structure of **2** is the same in both solvents. This suggests that the dimer is retained in solution, even in THF, a known coordinating solvent. In addition, the complexity of the spectrum (~ 30 lines) is consistent with a C_1 symmetric dimer. A C_s symmetric monomer would only display 16 resonances in the ^1H NMR spectrum, as is observed for the starting bromide **1**. The hydrides are not observed due to the extremely rapid relaxation experienced during the NMR experiment, a consequence from being directly bonded to the iron center.²⁵ Furthermore, no signals are observed when performing a standard $^{31}\text{P}\{^1\text{H}\}$ NMR experiment. Additional evidence for the dimeric structure of **2** is the low solution magnetic moment of $4.2\ \mu_{\text{B}}$ measured by the Evans method at $25\text{ }^{\circ}\text{C}$, indicating strong anti-ferromagnetic coupling of the normally high-spin Fe(II) centers in the dimer. Similarly low magnetic values have been reported for $[(^{\text{tBu}}\text{Nacnac}^{\text{DIPP}})\text{FeH}]_2$ at $25\text{ }^{\circ}\text{C}$.⁹

The synthesis of **2** must be performed at $-35\text{ }^{\circ}\text{C}$ to prevent a side reaction with the triethylborane byproduct. When **1** is treated with KBET_3H at $25\text{ }^{\circ}\text{C}$ and the reaction mixture is left to stir for 15 min, the ^1H NMR spectrum obtained for the product mixture contains 52 resonances. Single crystals picked from this reaction mixture were analyzed by X-ray diffraction and found to be the iron diethylhydridoborate complex **3** (see Figure S1 in the Supporting Information), which was produced in the reaction. The formation of **3** follows from the reaction of **2** with the byproduct triethylborane produced in the hydride metathesis reaction, which by mass balance should also generate the three-coordinate iron ethyl complex **4** (Scheme 1).

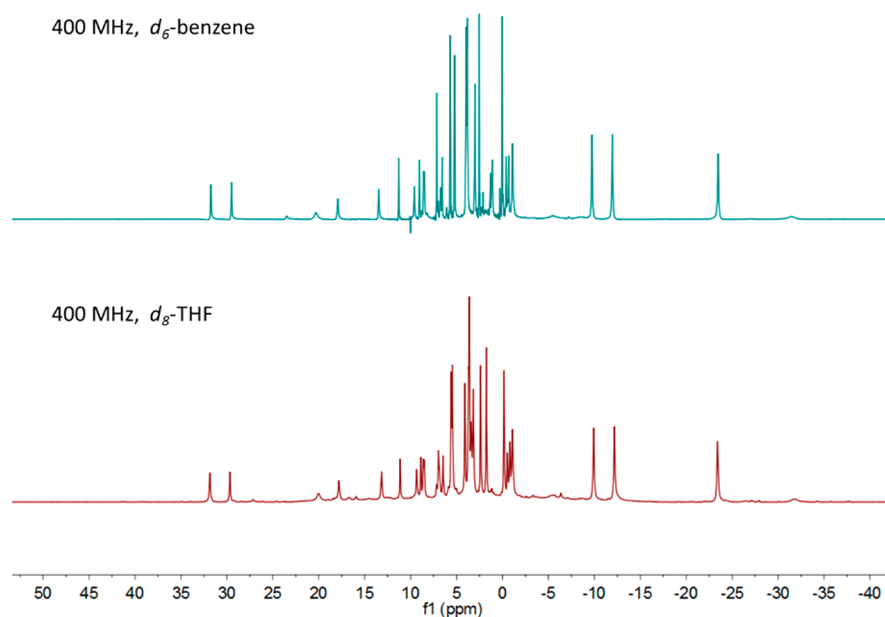
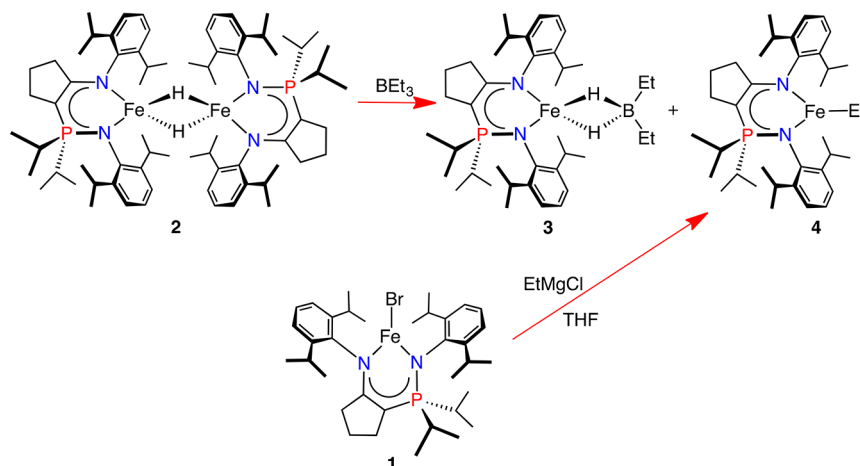


Figure 2. ^1H NMR spectra for $[(^{\text{CYS}}\text{NpN}^{\text{DIPP,DIPP}})\text{FeH}]_2$ **2** in d_6 -benzene (top) and d_8 -THF (bottom). Both spectra were collected at 400 MHz at $25\text{ }^{\circ}\text{C}$.

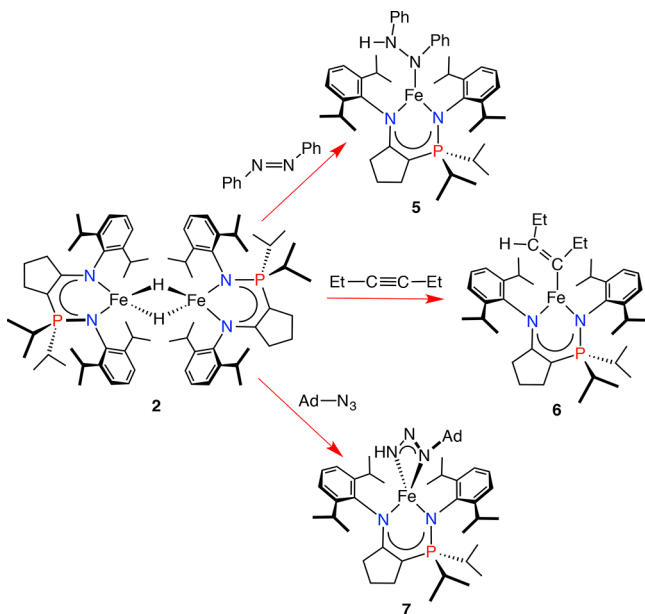
Scheme 1. Side Reaction of Hydride 2 with Triethylborane to Form 3 and 4; Synthesis of 4 from 1



To confirm that the iron ethyl species 4 was produced concurrently with complex 3, the bromide complex 1 was treated with ethylmagnesium chloride in THF, which cleanly produced 4. Comparison of the ¹H NMR spectrum of 4 to that obtained by reaction of 2 with BEt₃ confirms that 4 is present along with other resonances likely attributable to 3 (see Supporting Information Figures S12 and S13). Analogous reactivity has been well-established for the reaction between [(^tBuNacnac^{DIPP})FeH]₂ and triethylborane.²⁶

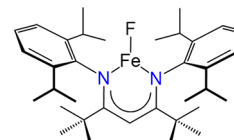
To probe the reactivity of our low-coordinate enamido-phosphinimine iron hydride system in comparison to the reactivity displayed by [(^tBuNacnac^{DIPP})FeH]₂, complex 2 was treated with a selection of substrates containing multiple-bond character (Scheme 2). In each case, the expected insertion

Scheme 2. Insertion Chemistry of Hydride 2 with Azobenzene, 3-Hexyne, and Adamantyl Azide



product was formed, with few differences in the structure of the resulting complex in comparison to the iron β-diketimate analogues.^{8,9} The insertion products were fully characterized; this information, including single-crystal X-ray structures, can be found in the Supporting Information (Figures S3–S5).

Catalytic Hydrodefluorination. The only reported example of iron-catalyzed hydro-defluorination utilizes the three-coordinate iron fluoride β-diketimate complex (^tBuNacnac^{DIPP})FeF in concert with Et₃SiH.²³ Table 1 presents

Table 1. Select Examples of Catalytic Hydrodefluorination^a Using an Iron(II) Fluoride Diketimate Complex

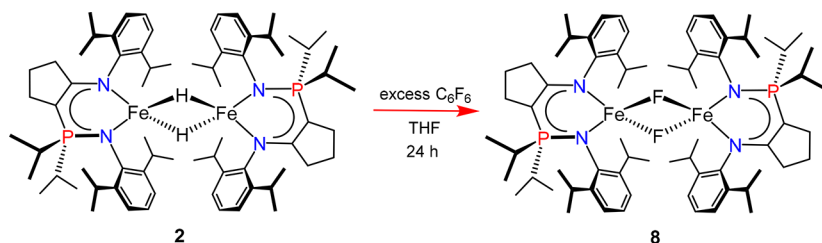
substrate	conditions	product distribution	TON
C ₆ F ₆	45 °C, 4 d	C ₆ HF ₅ (50%)	2.5
C ₅ F ₅ N	45 °C, 4 d	<i>p</i> -C ₅ HF ₄ N (71%)	3.6
C ₆ F ₅ CF ₃	45 °C, 12 h	<i>p</i> -C ₆ HF ₄ CF ₃ (90%)	4.5

^aEach reaction was run in *d*₈-THF using 20 mol % of catalyst; triethylsilane was used as a hydride source.

some selected examples using this Nacnac-based iron system in HDF of hexafluorobenzene (C₆F₆) to generate pentafluorobenzene (C₆F₅H), pentafluoropyridine (C₅F₅N) to generate *p*-tetrafluoropyridine (*p*-C₆F₄HN), and octafluorotoluene (C₆F₅CF₃) to give *p*-heptafluorotoluene (*p*-C₆F₄HCF₃).

Presumably, these HDF reactions operate via formation of a low-coordinate transient iron hydride species, which upon interaction with the fluorinated aromatic compound regenerates the iron fluoride species. However, there is no direct reaction between the hydride [(^tBuNacnac^{DIPP})FeH]₂ and C₆F₆ or octafluorotoluene (C₆F₅CF₃) even when heated to 120 °C in *d*₆-benzene or *d*₈-THF. Interestingly, in the presence of Et₃SiH, heating [(^tBuNacnac^{DIPP})FeH]₂ with C₆F₆ or C₆F₅CF₃ does result in the catalytic production of monodefluorinated products, though conversions are lower than when catalysis is performed with the iron fluoride as the precatalyst.²³

In contrast, the dinuclear dihydride 2 reacts directly with C₆F₆ in *d*₈-THF, with the formation of C₆F₅H observed by ¹⁹F NMR spectroscopy. The production of C₆F₅H is observed in as little as 15 min when heated to 70 °C, though decomposition of the iron-containing product also occurred at this temperature, as determined by ¹H NMR spectroscopy (Supporting Information Figures S15 and S14, respectively). If 2 reacts directly with C₆F₆ to generate C₆F₅H, it follows that

Scheme 3. Formation of Fluoride Dimer 8 by Reaction of C₆F₆ with Hydride 2

the concurrent formation of an iron fluoride species occurs. Reaction of **2** with excess C₆F₆ in THF overnight at room temperature afforded the isolation of the dimeric iron fluoride complex [(^{CY5}NpN^{DIPP,DIPP})FeF]₂ **8** (Scheme 3). The use of THF as the solvent is crucial for this reaction; attempting the reaction in diethyl ether or aromatic solvents failed to facilitate a reaction between **2** and C₆F₆.

The solid-state molecular structure for **8** is shown in Figure 3. The dimeric nature of **8** is somewhat surprising, as this previously

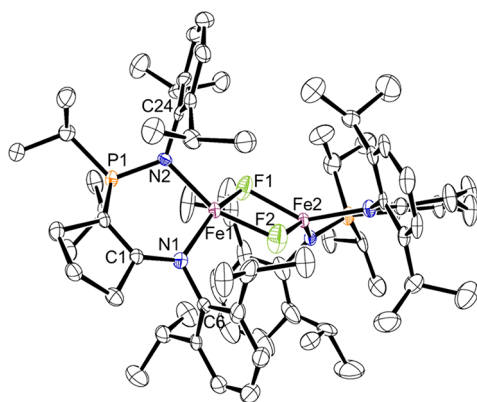


Figure 3. ORTEP drawing of the solid-state molecular structure of **8** (ellipsoids at 50% probability level). All hydrogen atoms were omitted for clarity. Selected bond lengths (Å) and angles (deg): Fe1–N1:2.055(5), Fe1–N2:2.058(5), Fe1–F1:2.033(4), Fe1–F2:1.990(4), Fe1–Fe2:3.1457(14), N1–Fe1–N2:96.5(2), F1–Fe1–F2:77.08(16), C1–N1–C6:114.3(5), and P1–N2–C24:123.1(4).

reported ligand has been used to prepare the three-coordinate iron bromide complex **1**.²⁴ A comparison of the angle between the nitrogen donors and the 2,6-diisopropylphenyl ring is used to quantify the difference in sterics between similar complexes. The C1–N1–C6 (114.3(5)°) and P1–N2–C24 (123.1(4)°) angles of **8** are shallower than the analogous angles found in **1** of 118.8(2)° and 125.9(2)°, respectively. Thus, a degree of flexibility exists in our enamido–phosphinimine ligand scaffold that is absent in the β-diketiminato systems. The C–N–C angles of 127.95(13)° found between the imine nitrogen and the aryl rings in the three-coordinate (^{tBu}Nacnac^{DIPP})FeF complex provide sufficient steric hindrance to force a trigonal planar geometry at the iron center. Interestingly, a less sterically hindered iron(II) fluoride complex featuring a β-diketiminato with methyl groups in the ligand backbone adopts a dimeric structure very similar to that of **8**. Thus, [(^{Me}Nacnac^{DIPP})FeF]₂ features C–N–C angles of 119.92(18)° and 117.32(18)° and an Fe–Fe distance of 3.0831(6) Å.²³ We suggest that the steric bulk imparted by our enamido–phosphinimine system is greater than the methyl-substituted Nacnac ligand but is less sterically hindered than the *tert*-butyl Nacnac scaffold.

The ¹H NMR spectrum for **8** contains 30 resonances, indicating that it exists as a dimer in solution. However, in contrast to **2**, the spectral window is more indicative of a monomeric species (with an extremely downfield-shifted resonance at δ 109.1). Fluoride ligands in linearly bridged species have been shown to allow weak anti-ferromagnetic exchange between paramagnetic metal centers.²⁷ Thus, the weak anti-ferromagnetism observed for dimeric **8** is likely a result of the bridging fluoride ligands. In agreement with this assessment is the relatively high solution magnetic moment of 6.2 μ_B per dimer at 25 °C, which is the same solution magnetic moment reported for dimeric [(^{Me}Nacnac^{DIPP})FeF]₂.²³ One final point is that, while we assume that **8** is the fluoro-bridged dimer, as one referee has pointed out, it could also be the hydroxo-bridged species [(^{CY5}NpN^{DIPP,DIPP})Fe(OH)]₂. The occupancies better match the fluoro derivative, but as discussed in the Experimental Section, without analytical data, the true identity is somewhat equivocal.

With reactivity between **2** and C₆F₆ established, catalytic HDF was investigated with the addition of Et₃SiH as the fluoride acceptor to the reaction mixture. Utilizing a catalyst loading of 0.05 mol equiv of **2** relative to equimolar amounts of C₆F₆ and Et₃SiH, catalytic mono-defluorination occurred in *d*₈-THF at 50 °C. A marginally higher TON of 4.2 was achieved under a shorter time period (2 d) relative to the HDF catalysis reported with the (^{tBu}Nacnac^{DIPP})FeF pre-catalyst with the same substrates (TON = 2.5, 4 d). Complex **2** also performs the mono-defluorination of 1,3,5-trifluorobenzene (C₆F₃H₃), though the TON is only 1.2 after 5 d at 70 °C. Interestingly, pre-catalyst **2** displays a higher tolerance to silane choice compared to the (^{tBu}Nacnac^{DIPP})FeF system, which is reported to decompose at room temperature in the presence of silanes other than Et₃SiH, such as triethoxysilane ((EtO)₃SiH) and triphenylsilane (Ph₃SiH). Both Ph₃SiH and butylsilane (*n*-BuSiH₃) can be utilized in the HDF of C₆F₆, albeit with lower conversions after a 2 d reaction period relative to using Et₃SiH as the fluoride acceptor (TON = 3 with Ph₃SiH and TON = 2.4 with *n*-BuSiH₃).

The greatest difference in reactivity between **2** and (^{tBu}Nacnac^{DIPP})FeF occurs in the HDF of C₅F₃N. After 3 d at 50 °C in *d*₈-THF, C₅F₃N was quantitatively converted to *p*-C₅HF₄N in the presence of **2**, when Et₃SiH is used as the fluoride acceptor (Figure 4). Higher TONs were achieved with lower catalyst loadings; for example, 0.01 mol equiv of **2** relative to C₅F₃N and Et₃SiH heated to 50 °C for one week resulted in 50% conversion to *p*-C₅HF₄N (TON = 50; Figure S29). This is a drastic difference in reactivity relative to (^{tBu}Nacnac^{DIPP})FeF, which is reported to have a TON of 3.6 for the HDF of C₅F₃N after 4 d at 45 °C. There does exist a similarity in the catalytic activity of both **2** and (^{tBu}Nacnac^{DIPP})FeF in that solvent choice is important for catalysis. For example, attempted HDF of C₆F₆ in *d*₆-benzene resulted in zero

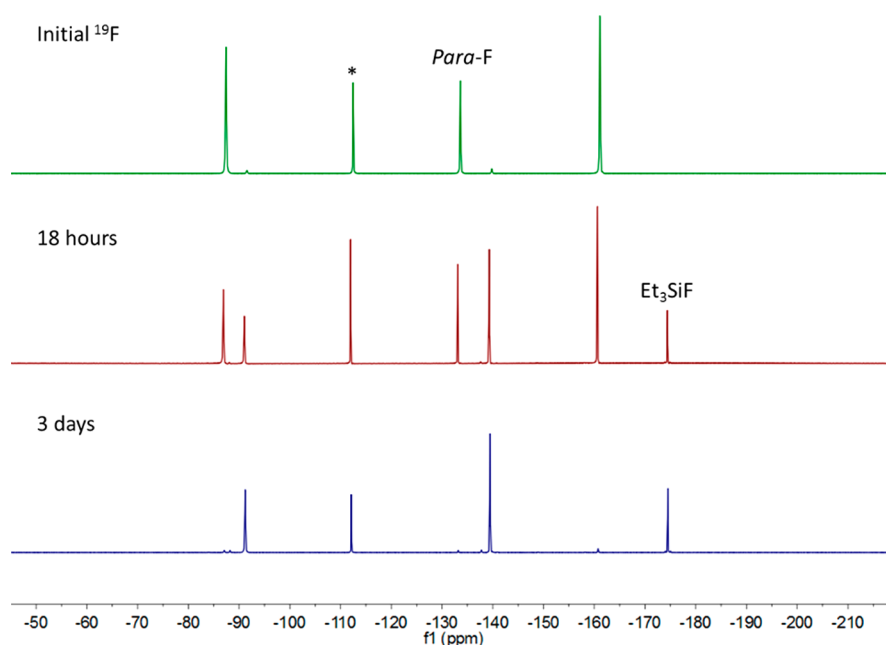


Figure 4. ^{19}F NMR for the catalytic HDF of pentafluoropyridine ($\text{C}_5\text{F}_5\text{N}$) using Et_3SiH as the fluoride trap and 5 mol % of **2** as the catalyst (d_8 -THF, $50\text{ }^\circ\text{C}$). After 18 h, the appearance of the *ortho* and *meta* ^{19}F resonances belonging to 2,3,5,6-tetrafluoropyridine ($p\text{-C}_5\text{HF}_4\text{N}$), along with the ^{19}F resonance for Et_3SiF , are observed. After 3 d, the resonance belonging to the *para*-F of $\text{C}_5\text{F}_5\text{N}$ is no longer observed, indicating complete consumption of $\text{C}_5\text{F}_5\text{N}$. Fluorobenzene was used as the internal standard and is denoted with *.

Table 2. Hydrodefluorination Results Utilizing the Iron(II) Hydride Complex **2 in Comparison to the Catalytic Activity of the β -Diketiminato Iron(II) Fluoride Catalyst**

precatalyst	substrate	reagent	solvent	conditions	TON
2 (5 mol %)	C_6F_6	Et_3SiH	d_8 -THF	$50\text{ }^\circ\text{C}/2\text{ d}$	4.2
2 (5 mol %)	$\text{C}_5\text{F}_5\text{N}$	Et_3SiH	d_8 -THF	$50\text{ }^\circ\text{C}/3\text{ d}$	20
2 (1 mol %)	$\text{C}_5\text{F}_5\text{N}$	Et_3SiH	d_8 -THF	$50\text{ }^\circ\text{C}/7\text{ d}$	50
2 (5 mol %)	$\text{C}_3\text{F}_3\text{H}_3$	Et_3SiH	d_8 -THF	$70\text{ }^\circ\text{C}/5\text{ d}$	1.2
2 (5 mol %)	C_6F_6	Et_3SiH	C_6D_6	$50\text{ }^\circ\text{C}/2\text{ d}$	0
2 (5 mol %)	C_6F_6	Et_3SiH	d_5 -pyridine	$50\text{ }^\circ\text{C}/2\text{ d}$	0
2 (5 mol %)	$\text{C}_5\text{F}_5\text{N}$	Et_3SiH	C_6D_6	$50\text{ }^\circ\text{C}/3\text{ d}$	11.2
2 (5 mol %)	C_6F_6	$n\text{-BuSiH}_3$	d_8 -THF	$50\text{ }^\circ\text{C}/2\text{ d}$	2.4
2 (5 mol %)	C_6F_6	Ph_3SiH	d_5 -THF	$50\text{ }^\circ\text{C}/2\text{ d}$	3
2 (5 mol %)	C_6F_6	Et_3SiH , DMAP	d_8 -THF	$50\text{ }^\circ\text{C}/2\text{ d}$	1.2
2 (5 mol %)	C_6F_6	Et_3SiH , PPh_3	d_3 -THF	$50\text{ }^\circ\text{C}/2\text{ d}$	5.4
($t\text{BuNacnacDIPP}$) FeF (20 mol %)	C_6F_6	Et_3SiH	d_8 -THF	$45\text{ }^\circ\text{C}/4\text{ d}$	2.5
($t\text{BuNacnacDIPP}$) FeF (20 mol %)	C_6F_6	Et_3SiH	C_6D_6	$45\text{ }^\circ\text{C}/4\text{ d}$	0.3
($t\text{BuNacnacDIPP}$) FeF (20 mol %)	$\text{C}_5\text{F}_5\text{N}$	Et_3SiH	d_8 -THF	$45\text{ }^\circ\text{C}/14\text{ d}$	3.6

production of $\text{C}_6\text{F}_5\text{H}$ when using **2** and marginal production in the case of ($t\text{BuNacnac}^{\text{DIPP}}$) FeF (TON = 0.3).²³ The use of d_6 -benzene as the solvent in the HDF of $\text{C}_5\text{F}_5\text{N}$ with **2** gave a reduced TON of 11.2 in contrast to the full conversion observed when d_8 -THF was the solvent. Thus, it is hypothesized that in both systems the presence of a coordinating solvent is necessary for either breaking up dimeric species during catalysis or stabilizing catalytic intermediates.

The observation that THF increased the catalytic activity of **2** toward HDF spurred the investigation into the addition of other donors to the catalytic defluorination of C_6F_6 in the presence of Et_3SiH . The addition of triphenylphosphine caused a marginally higher TON (5.4 with PPh_3 relative to TON = 4.2 without PPh_3), though the ^1H NMR spectrum of the iron-containing resting state indicates that the phosphine is not coordinated. Interestingly, the addition of 4-dimethylaminopyridine (DMAP) to the reaction mixture or using d_5 -pyridine as the solvent entirely arrests HDF catalysis. It is reasonable to

suggest that the presence of a weakly coordinating ligand aids in breaking apart the iron hydride dimer and facilitates reactivity, but too strong of a donor inhibits catalysis, likely through occupation of coordination sites necessary for reactivity. A summary of the catalysis results discussed above are shown in Table 2.

As solvent choice plays an important role in HDF catalysis, we postulated the structure of the operative species as the monomeric form of **2** and sought to detect this species at higher temperatures. Heating a d_8 -THF solution of **2** to $60\text{ }^\circ\text{C}$ only afforded small changes in the ^1H NMR spectrum (see Figure S38 in Supporting Information). Upon close inspection of the ^1H NMR spectrum at $60\text{ }^\circ\text{C}$, a new set of resonances at δ 37.3 and 35.4 are apparent. Cooling the NMR sample from 60 to $25\text{ }^\circ\text{C}$ resulted in the disappearance of these two signals. This suggests that, at elevated temperature, dimeric **2** may exist in equilibrium with its monomeric form (Supporting Information Figure S39).

Having established catalytic activity for the hydride complex **2**, we turned our attention to whether the dimeric iron

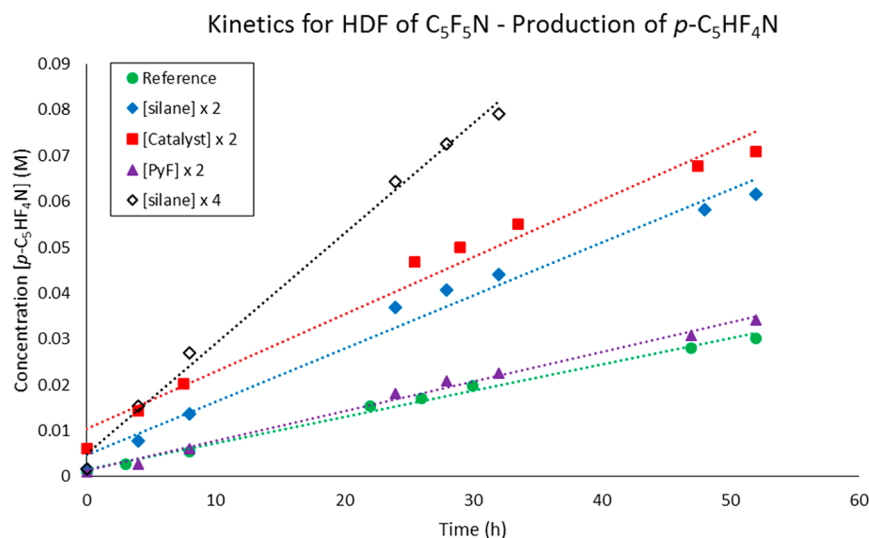


Figure 5. Progress of HDF for pentafluoropyridine showing the changes in rate due to changes in substrate concentration relative to a reference experiment with $[\text{silane}] = [\text{PyF}] = 0.11 \text{ M}$, $[\text{Fe}] = 5.5 \times 10^{-3} \text{ M}$ using d_8 -THF at $50 \text{ }^\circ\text{C}$.

fluoride species **8** could also participate in catalytic HDF. Unfortunately, employing the same conditions used for the HDF of C_6F_6 with **2** does not result in catalysis when starting with 5 mol % of **8** (TON = 0.8). The inactivity of fluoride **8** in comparison to the hydride **2** is somewhat puzzling, and stands in contrast to the reactivity observed for the β -diketiminato system.²³ We suggest these differences arise from distinct solution-state equilibria for the dissociation of dimeric species in THF. Further support for this hypothesis is illustrated by the lack of HDF activity reported for the analogous dimeric β -diketiminato iron fluoride $[(^{\text{Me}}\text{Nacnac}^{\text{DIPP}})\text{FeF}]_2$.²³ An examination of the reaction kinetics and ^1H NMR spectra collected during catalysis provides some insight into potential mechanistic pathways.

Mechanistic Considerations. A series of kinetic experiments were performed for the HDF of pentafluoropyridine at $50 \text{ }^\circ\text{C}$ using precatalyst **2** and Et_3SiH as the fluoride acceptor (Figure 5 and Table 3). The production of 2,3,5,6-tetrafluoropyridine and

Table 3. Parameters for Kinetic Investigation of Pentafluoropyridine HDF

entry	$[\text{Et}_3\text{SiH}]$ (M)	$[\text{C}_5\text{F}_5\text{N}]$ (M)	[2] (M)	rate ($1 \times 10^{-7} \text{ M s}^{-1}$)
reference	0.11	0.11	5.5×10^{-3}	1.6(1)
$[\text{silane}] \times 2$	0.22	0.11	5.5×10^{-3}	3.2(2)
$[\text{catalyst}] \times 2$	0.11	0.11	0.011	3.5(2)
$[\text{PyF}] \times 2$	0.11	0.22	5.5×10^{-3}	1.8(1)
$[\text{silane}] \times 4$	0.44	0.11	5.5×10^{-3}	6.7(3)

fluorotriethylsilane was monitored by quantitative ^{19}F NMR spectroscopy over the course of 2 d. Because of the stability of the starting iron hydride catalyst, the course of the reaction could be monitored over this time frame, as the rate of reaction remained relatively constant. From a comparison of the reaction rates for the various kinetic runs, it can be seen that the reaction is first-order with respect to both the iron hydride **2** and Et_3SiH but is zero order with respect to pentafluoropyridine. The general rate law is shown in eq 2:

$$\frac{d[p\text{-C}_5\text{HF}_4\text{N}]}{dt} = k[\text{Et}_3\text{SiH}]^1[\mathbf{2}]^1[\text{C}_5\text{F}_5\text{N}]^0 \quad (2)$$

The second-order rate constant obtained from this equation is $k = 2.8(1) \times 10^{-4} \text{ s}^{-1} \text{ M}^{-1}$. This rate law obtained for HDF of $\text{C}_5\text{F}_5\text{N}$ using **2** is identical to that reported by Holland and co-workers for the hydro-defluorination of octafluorotoluene using the $(^{\text{tBu}}\text{Nacnac}^{\text{DIPP}})\text{FeF}$ catalyst.²³

Comparable reaction rates are observed for the production of Et_3SiF , with the only difference being the initial production of $p\text{-C}_5\text{HF}_4\text{N}$ for the trial where the concentration of **2** was doubled (Supporting Information Figure S42). The initial amount of $p\text{-C}_5\text{HF}_4\text{N}$ produced at $t = 0$ for $[\text{catalyst}] \times 2$ is double that of the reference trial, whereas initial production of Et_3SiF for both the reference trial and $[\text{catalyst}] \times 2$ is zero. This observation is in agreement with the derived rate law, in which the iron hydride **2** quickly reacts with $\text{C}_5\text{F}_5\text{N}$ and the rate-limiting step in catalysis involves the silane.

Examination of the ^1H NMR spectra collected during the various catalytic trials provides some insight into the identity of the paramagnetic resting state. As seen in Figure 6, the paramagnetic species observed during each of the HDF catalytic trials remains unchanged regardless of the fluorinated substrate or silane utilized. The ^1H NMR spectrum obtained from the trial using $n\text{-BuSiH}_3$ as the fluoride acceptor did contain additional resonances not observed in the trials using Et_3SiH or Ph_3SiH , but the major species present is consistent with that observed in the other trials. Likewise, the same paramagnetic species is present in both the HDF catalysis for C_6F_6 and $\text{C}_5\text{F}_5\text{N}$, indicating that the resting state does not have the fluorinated substrate coordinated to iron. As neither the identity of the fluorinated substrate nor the silane changes the paramagnetic resting state, we wondered if the species is the iron fluoride complex **8**. However, comparison of the ^1H NMR spectra for **2**, **8**, and the resting states obtained from HDF of C_6F_6 with Et_3SiH utilizing **2** and **8** as precatalysts rules out **2** and **8** as the resting state (Figure S41 in Supporting Information).

Interestingly, stepwise progression of HDF can be observed through sequential addition of reagents. When 1 equiv of C_6F_6 is added to a d_8 -THF solution of **2** and heated to $50 \text{ }^\circ\text{C}$ for 1 d, nearly quantitative consumption of hydride dimer **2** was achieved with concurrent formation of the catalytic resting state, as observed by ^1H NMR spectroscopy. The addition of 1 equiv of Et_3SiH to this solution followed by heating to $50 \text{ }^\circ\text{C}$

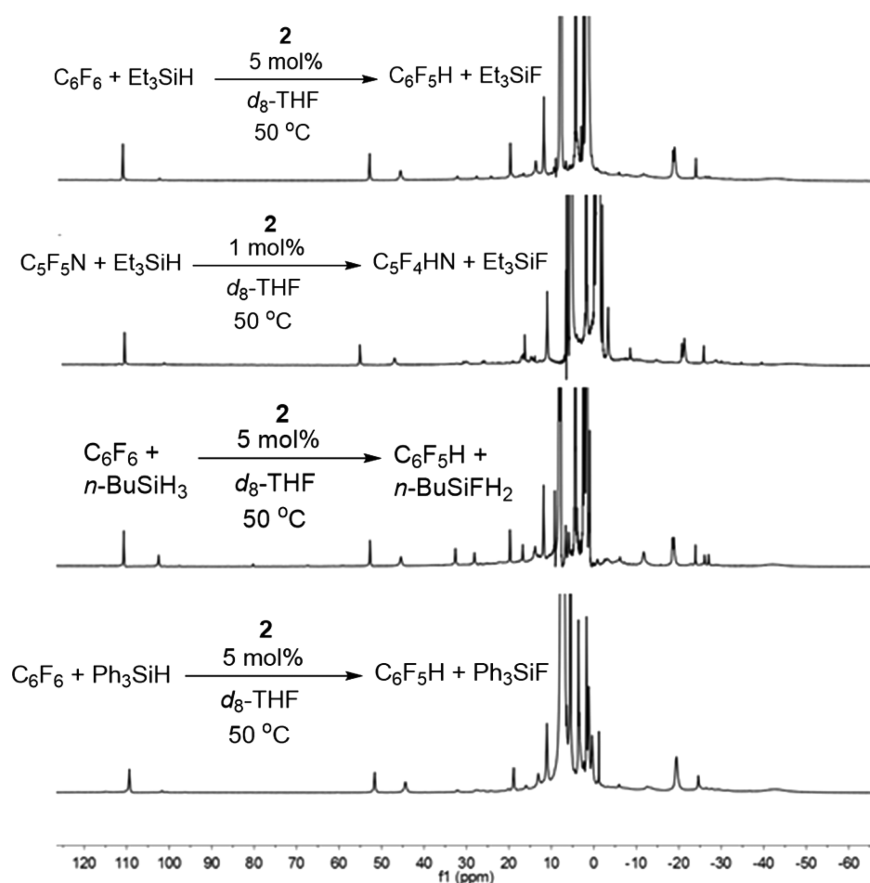


Figure 6. A comparison of the ^1H NMR spectra collected at the final time points of various HDF catalytic runs using different substrates. With the exception of the trial utilizing *n*-BuSiH₃ as the fluoride acceptor, all observed resonances are consistent between trials. This indicates that the resting state during catalysis does not depend on the fluorinated substrate. All spectra collected in *d*₈-THF at 300 MHz at 25 °C.

for an additional day allows for the partial conversion of the catalytic resting state back to **2**, seen in Figure 7.

To further understand the energetics of iron-based HDF catalysis, the energy barriers associated with proposed catalytic transition states were calculated and compared for both Nacnac and NpN iron complexes.

DFT Calculations. A proposed catalytic cycle for the HDF of C_6F_6 in the presence of Et_3SiH is shown below in Scheme 4. While the monomers of complexes **2** and **8** are depicted in Scheme 4, analogous species featuring the ^{tbu}Nacnac^{DIPP} ligand are applicable. Each minimum was optimized at the B3LYP/6-311+G(d) level of theory starting from the solid-state molecular structure, and all were found to be a local energetic minimum. Transition states were located using the Gaussian09 implementation of the Berny algorithm.²⁸ All final energy values were determined using the 6-311G(d) basis set^{29–33} and the B3LYP functional.^{34–37} The connectivity of transition states and minima were found using intrinsic reaction coordinate (IRC) calculations. Figure 8 shows a comparison of the energy of each transition state relative to LFeH , Et_3SiH , and C_6F_6 for both the NpN and Nacnac systems. The activation energy for step A (Fe–H adduct formation with C_6F_6) is lower for the NpN system than for the Nacnac analogue by ~ 5 kJ/mol, while step C (Fe–F adduct formation with Et_3SiH) is ~ 30 kJ/mol higher for NpN in comparison to the Nacnac case. The magnitude of the calculated energy values are not an accurate representation of the differences in reactivity when comparing low-coordinate iron hydride and fluoride complexes of NpN to

Nacnac, but the overall trend in energy values is consistent with experimental observations. That is, process A is facile for the iron hydride **2**, but it is reported to not take place for $[(^{\text{tbu}}\text{Nacnac}^{\text{DIPP}})\text{FeH}]_2$. Likewise, complex **8** did not serve as a precatalyst for HDF, but reactivity is observed for $(^{\text{tbu}}\text{Nacnac}^{\text{DIPP}})\text{FeF}$. Thus, the proposed catalytic cycle is thermodynamically feasible, but in reality HDF catalysis via low-coordinate iron complexes is likely a more complicated process than what is described here.

CONCLUSION

The dimeric iron(II) hydride species **2** bearing the enamido-phosphinimine ligand scaffold was successfully synthesized by treatment of the iron bromide complex **1** with KBET_3H . Complex **2** reacted with the unsaturated substrates azobenzene, 3-hexyne, and 1-azidoadamantane to yield the expected insertion products. Surprisingly, **2** displayed reactivity toward the fluorinated aromatic compounds C_6F_6 and $\text{C}_5\text{F}_5\text{N}$. Single crystals of the iron fluoride complex **8** were isolated from the reaction of **2** with C_6F_6 . This stands in contrast to the lack of reactivity that the β -diketiminate iron hydride systems display toward fluorinated aromatics. HDF catalysis was performed using 5 mol % loadings of precatalyst **2**, and a variety of silanes can act as fluoride acceptors without catalyst decomposition. The highest TON of 50 was observed for the HDF of $\text{C}_5\text{F}_5\text{N}$ (1 mol % loading **2**). Kinetic experiments highlighted the stability of the active catalytic species, as reaction rates were relatively linear over the course of 50 h. The general rate law for HDF of $\text{C}_5\text{F}_5\text{N}$ with precatalyst **2** was in agreement with the

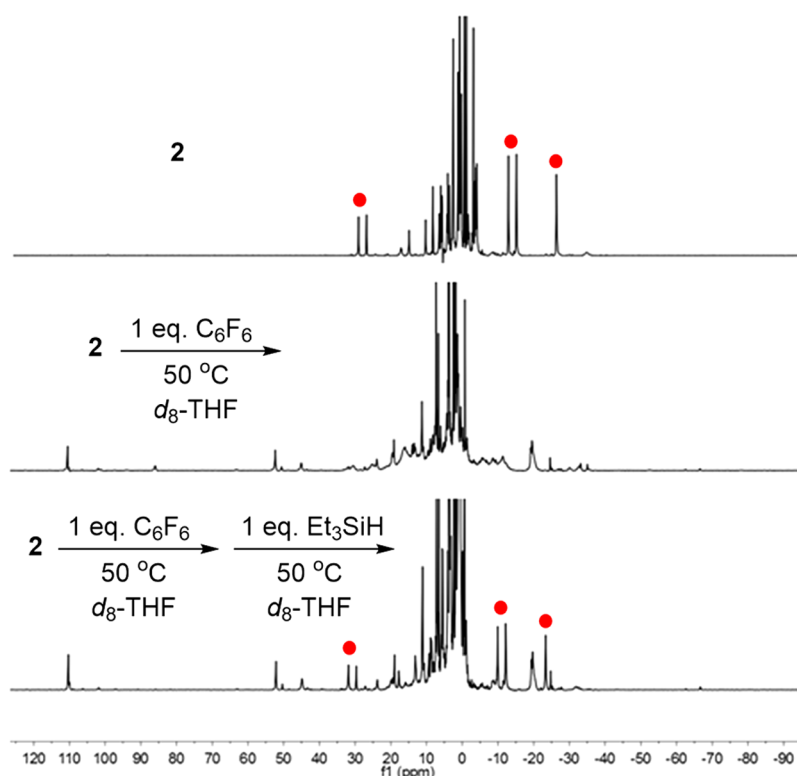
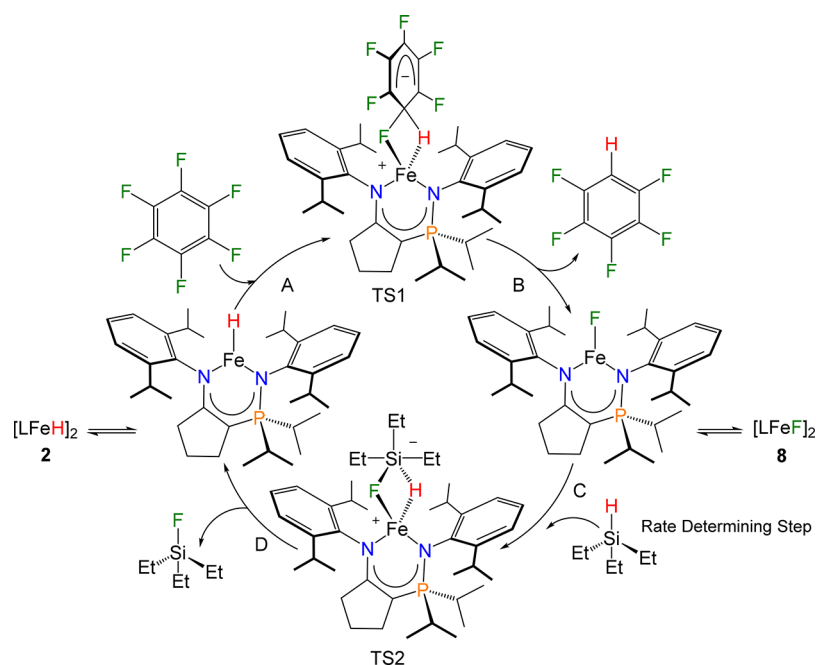


Figure 7. ^1H NMR spectra for **2** (top), the reaction between **2** and C_6F_6 (middle), and the subsequent reaction with Et_3SiH (bottom). (red ●) Resonances belonging to the hydride **2** are observed following the reaction with Et_3SiH . All spectra collected in d_8 -THF at 300 MHz at 25 °C.

Scheme 4. Proposed Catalytic Cycle for the Hydrodefluorination of C_6F_6



rate law for HDF catalysis of $\text{C}_6\text{F}_5\text{CF}_3$ reported for the (^tBu NacNac^{DIPP})FeF system. Both systems display a first-order dependence on silane concentration, indicating that the reaction of a low-coordinate iron fluoride with silane is the rate-determining step in HDF. However, the ^1H NMR spectra obtained for the catalytic resting states across multiple trials does not agree with the spectrum for **8**, making a definitive claim as to the identity of the resting state difficult.

The possibilities for improvements to catalytic rate and turnover are numerous and could potentially be achieved through further steric modification of the enamido–phosphinimine scaffold.

EXPERIMENTAL SECTION

General Considerations. All manipulations were performed under an atmosphere of dry and oxygen-free dinitrogen (N_2) by means of standard Schlenk or glovebox techniques. Anhydrous THF,

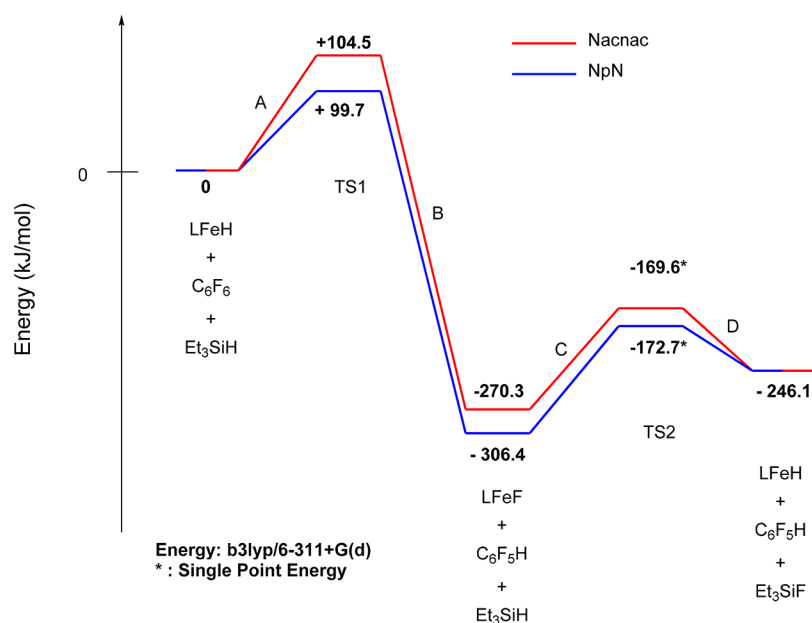


Figure 8. Computational analyses of one HDF cycle to compare the relative energies of the Nacnac-iron system (red) to the NpN-iron system (blue).

toluene, Et₂O, and hexanes were purchased from Aldrich, sparged with N₂, and dried further by passage through towers containing activated alumina and molecular sieves. Benzene-*d*₆ was refluxed over sodium, vacuum transferred, and freeze–pump–thaw degassed. THF-*d*₈ was purchased from Aldrich (≥99.5% atom % D) in 1 mL ampules and was dried over activated 4 Å molecular sieves. ¹H and ¹⁹F NMR spectra were recorded on a Bruker AV-300 MHz spectrometer or a Bruker AV-400 MHz spectrometer. Unless noted otherwise, all spectra were recorded at room temperature. ¹H NMR spectra were referenced to the residual proton signal in *d*₆-benzene (7.16 ppm) or *d*₈-THF (1.72 ppm); ¹⁹F NMR spectra were referenced to fluorobenzene at –113.15 ppm. Evans NMR spectroscopy was performed by measuring the shift in frequency for the ¹H NMR signal of cyclooctane in a sealed capillary containing 1 mol % cyclooctane in *d*₆-benzene relative to a 1 mol % cyclooctane in *d*₆-benzene solution containing the desired paramagnetic compound. The Evans measurements were collected at 25 °C. Microanalyses (C, H, N) were performed at the Department of Chemistry at the University of British Columbia. Low- and high-resolution mass spectrometry was performed with a Kratos MS 50 at the University of British Columbia.

Suitable single crystals were selected in a glovebox, coated in Fomblin oil, and mounted on a glass loop. X-ray data were collected on a Bruker X8 Apex II diffractometer with a graphite-monochromated Mo K α radiation ($\lambda = 0.71073$ Å) at a temperature of 90 K. Data were collected and integrated using the Bruker SAINT software package.³⁸ Absorption corrections were performed using the multiscan technique (SADABS).³⁹ All structures were solved by direct methods and refined using the Olex2 (version 1.2.5) software package⁴⁰ and the ShelXL refinement program.⁴¹ All non-hydrogen atoms were refined anisotropically. ORTEPs were generated using ORTEP-3 (version 2.02).⁴²

The syntheses for the iron bromide complex **1** has been previously reported.²⁴ Potassium triethylborohydride was purchased as a 1.0 M solution in THF from Sigma-Aldrich and was dried under vacuum, affording a crystalline solid that was stored and used in the N₂ glovebox. Hexafluorobenzene, fluorobenzene, 1,3,5-trifluorobenzene, pentafluoropyridine, triethylsilane, butylsilane, and 3-hexyne were degassed and stored over activated molecular sieves before use. 1-Azidoadamantane, azobenzene, and triphenylsilane were degassed under vacuum and used within the N₂ glovebox. Ethylmagnesium chloride was purchased as a 2.0 M solution in THF from Sigma-Aldrich and was used as received.

Computations. All atoms were described with a 6-311G(d) triple- ζ basis set.^{29–33} Calculations were performed at the DFT level of theory using the hybrid functional B3LYP.^{34–37} Geometry optimizations were

performed without any symmetry restrictions, and the nature of the extremes (minima and transition states) was verified with analytical frequency calculations. Gibbs free energies were obtained at $T = 298.15$ K within the harmonic approximation. IRC calculations were performed to confirm the connections of the optimized transition states. DFT calculations were performed with the Gaussian09 suite of programs.²⁸ Calculations were realized in the gas phase, and the real NpN and Nacnac ligands were computed.

Syntheses. [(^{CY5}NpN^{DIPP,DIPP})FeH]₂ **2**. The previously reported complex **1** (0.242 g, 0.361 mmol) and potassium triethylborohydride (0.050 g, 0.361 mmol) were each dissolved separately in toluene (5 mL), and the two solutions were cooled to –35 °C in the glovebox freezer. The cooled solution of KBH₃Et₃ was quickly added to the cooled solution of **1** while the mixture was stirred with a magnetic stir bar. The reaction mixture rapidly changed color from yellow-orange to dark brown and was allowed to stir for 3 min before being filtered through a filter pipet packed with diatomaceous earth to remove the KBr byproduct. The filtrate was dried under vacuum, and the resulting residue was redissolved in Et₂O and again dried to give the product as an orange-brown powder. Yield: 0.161 g, 0.136 mmol, 75.6%. Single crystals of **2** suitable for X-ray diffraction were grown from a toluene solution cooled to –35 °C. ¹H NMR (400 MHz, *d*₆-benzene, 25 °C): δ 31.8, 29.5, 23.4, 20.3, 17.9, 13.6, 11.3, 9.6, 9.0, 8.5, 6.7, 6.6, 5.7, 5.2, 4.0, 3.8, 3.0, 2.6, 1.3, 1.1, –0.0, –0.3, –0.7, –1.2, –5.5, –8.6, –9.7, –11.9, –23.5, and –31.6. $\mu_{\text{eff}} = 4.2 \mu_{\text{B}}$ (Evans). Anal. Calcd for C₇₀H₁₁₀Fe₂N₄P₂: C, 71.17; H, 9.39; N, 4.74. Found: C, 71.33; H, 9.52; N, 4.61%.

(^{CY5}NpN^{DIPP,DIPP})FeEt **4**. The iron bromide complex **1** (0.190 g, 0.284 mmol) was dissolved in THF (10 mL) and was transferred to a Schlenk vessel. A solution of ethylmagnesium chloride (2.0 M in THF, 0.14 mL, 0.284 mmol) was added via syringe to the solution of **1**. The color of the reaction mixture immediately changed from yellow to brown/green. The reaction mixture was allowed to stir for 1 h before the volatiles were removed under vacuum and the Schlenk vessel was transferred into a dinitrogen glovebox. The residue in the Schlenk flask was dissolved in minimal diethyl ether and was filtered through a glass fiber filter pad to remove the MgBrCl byproduct. The filtrate was again dried under vacuum, yielding the product as a yellow powder. Yield: 0.077 g, 0.124 mmol, 44.0%. Single crystals suitable for X-ray diffraction were grown from slow evaporation of a diethyl ether solution of **4**. ¹H NMR (300 MHz, *d*₆-benzene, 25 °C): δ 96.8, 36.3, 26.9, 25.7, 24.7, 12.7, 12.1, 3.8, 1.8, 1.3, 0.3, –3.5, –20.9, –26.6, –30.3, –33.3, and –35.8. $\mu_{\text{eff}} = 4.0 \mu_{\text{B}}$ (Evans). High-resolution mass spectrometry (HRMS) (EI-Double Focusing Sector) m/z : [M]⁺ Calcd for

$C_{37}H_{59}N_2PF_6$: 618.376 53; Found: 618.376 68, $[M-CH_2CH_3]^+$ Calcd for $C_{35}H_{54}N_2PF_6$ 589.337 40; Found: 589.337 15.

$(^{CY5}NpN^{DIPP,DIPP})Fe(N(Ph)NHPPh)$ 5. A THF solution (5 mL) of complex 2 (0.075 mg, 0.127 mmol) was added to a THF solution (5 mL) of azobenzene (0.023 g, 0.127 mmol). The resulting dark red reaction mixture was stirred for 5 min before exposing the sample to vacuum to remove the volatiles. Yield: 0.094 g, 0.122 mmol, 96.1%. Single crystals suitable for X-ray diffraction were grown from the slow evaporation of a diethyl ether solution of 5. 1H NMR (300 MHz, d_6 -benzene, 25 °C): δ 112.0, 108.6, 107.3, 61.9, 40.4, 37.5, 26.3, 25.1, 23.4, 20.0, 19.0, 17.6, 14.3, 13.2, 8.0, 3.6, 1.4, 0.3, -0.6, -1.8, -3.2, -5.3, -9.0, -10.9, -13.0, -16.4, -18.8, -23.1, -27.3, -28.3, -31.4, -39.7, and -59.3. $\mu_{eff} = 4.1 \mu_B$ (Evans). Anal. Calcd for $C_{47}H_{65}FeN_4P$: C, 73.04; H, 8.48; N, 7.25. Found: C, 70.84; H, 8.47; N, 7.10%. Repeated attempts at elemental analysis failed to provide successful results. The analogous iron hydrazido β -diketiminato complex has been reported to be too thermally sensitive to provide satisfactory elemental analysis results.⁹

$(^{CY5}NpN^{DIPP,DIPP})Fe(3\text{-hexene})$ 6. Complex 2 (0.070 g, 0.118 mmol) was dissolved in THF (5 mL), and to the stirred solution was added excess 3-hexyne (0.015 g, 0.183 mmol). The reaction mixture was stirred overnight at room temperature, with the color of the solution gradually changing from orange to yellow over the course of the reaction. The volatiles were then removed under vacuum, leaving the product as a yellow powder. Yield: 0.066 g, 0.098 mmol, 82.5%. Single crystals suitable for X-ray diffraction were grown from the slow evaporation of a diethyl ether solution of 6. 1H NMR (300 MHz, d_6 -benzene, 25 °C): δ 98.7, 32.7, 27.2, 26.0, 25.1, 16.7, 15.3, 10.4, 2.9, 2.1, 1.2, -3.4, -22.0, -23.1, -25.4, -29.0, -34.9, and -36.0. $\mu_{eff} = 4.8 \mu_B$ (Evans). HRMS (EI-Double Focusing Sector) m/z : $[M]^+$ Calcd for $C_{41}H_{65}N_2PF_6$: 672.423 48; Found: 672.423 06.

$(^{CY5}NpN^{DIPP,DIPP})Fe(\eta^2\text{-HNNAd})$ 7. Complex 2 (0.063 g, 0.107 mmol) was dissolved in diethyl ether (5 mL) and was added to 1-azidoadamantane (0.019 g, 0.107 mmol), and the resulting mixture was stirred overnight at ambient temperature. The volatiles were then removed under vacuum, yielding the product as a brown powder. Yield: 0.070 g, 0.091 mmol, 85.4%. Single crystals suitable for X-ray diffraction were grown from a toluene solution of 7 cooled to -35 °C. 1H NMR (400 MHz, d_6 -benzene, 25 °C): δ 96.0, 30.6, 26.4, 23.5, 12.0, 11.3, 8.8, 8.2, 6.1, 5.2, 4.6, 3.3, 2.3, 1.9, 1.3, 1.1, -2.0, -3.2, -4.7, -6.1, -8.6, -11.2, -17.2, and -18.8. $\mu_{eff} = 4.3 \mu_B$ (Evans). Anal. Calcd for $C_{45}H_{70}FeN_5P$: C, 70.39; H, 9.19; N, 9.12. Found: C, 70.52; H, 9.46; N, 6.72%. Repeated attempts at elemental analysis consistently yielded results low in nitrogen. The β -diketiminato iron triazenido analogue to 7 is reported to be too thermally unstable to obtain accurate elemental analysis results.⁸

$[(^{CY5}NpN^{DIPP,DIPP})FeF_2]$ 8. Hexafluorobenzene (1.960 g, 10.5 mmol) was added to a THF solution (10 mL) of 2 (0.140 g, 0.237 mmol). The mixture was allowed to stir for 18 h at ambient temperature with the color of the solution gradually changing from orange to yellowish-green. The volatiles were removed under vacuum, yielding the product as a flaky yellow-green solid. Yield: 0.137 g, 0.225 mmol, 95.1%. Single crystals suitable for X-ray diffraction were grown from a toluene solution of 9 cooled to -35 °C. 1H NMR (300 MHz, d_6 -benzene, 25 °C): δ 109.1, 89.2, 81.7, 51.0, 48.6, 40.6, 37.7, 26.4, 23.1, 19.2, 16.3, 14.6, 10.7, 8.8, 6.4, 4.5, 2.3, 1.2, -0.7, -7.7, -9.3, -13.2, -16.7, -20.4, -23.1, -24.1, -28.5, -30.2, -52.8, and -66.7. $\mu_{eff} = 6.2 \mu_B$ (Evans).

Many attempts at obtaining elemental analyses were made, without success. We also tried to obtain EI mass spectra without success. As one referee pointed out, this complex could also be the hydroxo-bridged derivative, $[(^{CY5}NpN^{DIPP,DIPP})Fe(OH)]_2$. While the refinement of the X-ray data better matched the fluoro-bridged species, the hydroxo-bridged species also has similar occupancies. Without acceptable elemental analytical data or mass spectra to back up the true identity of 8, we concur that either formulation is possible.

Reaction of 2 with Triethylborane. Hydride complex 2 (0.008 g, 0.013 mmol) was dissolved in d_8 -toluene (0.6 mL) and was transferred to a J. Young NMR tube. The tube was charged with 1 M triethylborane in hexanes (13.6 μ L, 0.013 mmol) before being sealed and heated to 60 °C for 2 h. 1H NMR spectroscopy was performed at

25 °C. 1H NMR (300 MHz, d_8 -toluene, 25 °C): δ 113.4, 109.0, 96.3, 40.2, 37.4, 31.5, 26.6, 25.5, 24.7, 22.8, 20.2, 19.9, 19.2, 16.3, 14.8, 12.8, 12.1, 9.4, 4.3, 2.9, 1.2, 0.9, -0.3, -3.5, -6.2, -8.5, -16.9, -20.8, -26.6, -30.3, -33.1, -35.8, and -36.4. Comparison to 4: 1H NMR (300 MHz, d_6 -benzene, 25 °C): δ 96.8, 26.9, 25.7, 24.7, 12.7, 12.1, 3.8, 1.8, 1.3, 0.3, -3.5, -20.9, -26.6, -30.3, -33.3, and -35.8.

HDF Catalysis. For each independent trial, 10–15 mg of 2 was weighed and dissolved in ~0.6 mL of deuterated solvent. The substrates under investigation were measured to be in excess, so that 2 would be at a catalyst loading of 5 mol %. Substrates were added via Hamilton syringe to the solution of 2 and the resulting solution was transferred into a J. Young NMR tube. The tube was heated to 50 °C and was monitored periodically by 1H and ^{19}F NMR spectroscopy.

Kinetics of Pentafluoropyridine HDF. A standard solution containing 2 and fluorobenzene in d_8 -THF ($[Fe] = 5.5 \times 10^{-3}$ M, $[C_6H_5F] = 0.11$ M) was used for each catalytic run. In each trial, a J. Young NMR tube was charged with 600 μ L of the d_8 -THF solution containing 2 and the C_6H_5F internal standard using a Hamilton syringe. The amount of pentafluoropyridine and triethylsilane for each trial was calculated and was measured with a Hamilton syringe and added to the J. Young tube. For the trial where $[Fe] \times 2$ was measured, a new solution with $[Fe] = 0.011$ M was prepared. Each tube was heated to 50 °C but was cooled to 25 °C when monitored using ^{19}F NMR spectroscopy. A relaxation delay of 70 s was used to ensure integration values were quantitative. Lines of best fit for $[p\text{-}C_5HF_4N]$ versus time were plotted using linear regression, and the error was calculated using Microsoft Excel's LINEST function.

Stepwise HDF Reactivity. A solution of 2 (0.010 g, 0.017 mmol) and hexafluorobenzene (2 μ L, 0.017 mmol) in d_8 -THF (0.6 mL) was transferred to a J. Young NMR tube. The tube was sealed and heated to 50 °C for 1 d before being monitored by 1H NMR spectroscopy. Triethylsilane (3 μ L, 0.019 mmol) was added to the solution, and the tube was heated for an additional 1 d at 50 °C before being monitored by 1H NMR spectroscopy.

■ ASSOCIATED CONTENT

📄 Supporting Information

The Supporting Information is available free of charge on the ACS Publications website at DOI: 10.1021/acs.inorgchem.7b02199.

Text, figures, and tables giving full experimental procedures, representative NMR spectra, crystallographic data, and additional kinetic data (PDF)

Accession Codes

CCDC 1570900–1570906 contain the supplementary crystallographic data for this paper. These data can be obtained free of charge via www.ccdc.cam.ac.uk/data_request/cif, or by emailing data_request@ccdc.cam.ac.uk, or by contacting The Cambridge Crystallographic Data Centre, 12 Union Road, Cambridge CB2 1EZ, UK; fax: +44 1223 336033.

■ AUTHOR INFORMATION

Corresponding Author

*E-mail: fryzuk@chem.ubc.ca. Fax: +1 604 822-2847. Phone: +1 604 822-2897.

ORCID

Michael D. Fryzuk: 0000-0002-3844-098X

Author Contributions

The manuscript was written through contributions of all authors.

Notes

The authors declare no competing financial interest.

■ ACKNOWLEDGMENTS

M.D.F. thanks the NSERC of Canada for a Discovery Grant.

REFERENCES

- (1) McWilliams, S. F.; Holland, P. L. Dinitrogen Binding and Cleavage by Multinuclear Iron Complexes. *Acc. Chem. Res.* **2015**, *48*, 2059–2065.
- (2) Holland, P. L. Distinctive Reaction Pathways at Base Metals in High-Spin Organometallic Catalysts. *Acc. Chem. Res.* **2015**, *48*, 1696–1702.
- (3) Vedernikov, A. N. Mechanism of the Kumada–Corriu Cross-Coupling Catalyzed by Low-Coordinate Bis(amido)–Nickel Complexes: Identification of Nickel(I)–(III) Catalytic Intermediates. *ChemCatChem* **2014**, *6*, 2490–2492.
- (4) Ung, G.; Peters, J. C. Low-Temperature N₂ Binding to Two-Coordinate L₂Fe⁰ Enables Reductive Trapping of L₂FeN₂[–] and NH₃ Generation. *Angew. Chem., Int. Ed.* **2015**, *54*, 532–535.
- (5) Monillas, W. H.; Yap, G. P. A.; MacAdams, L. A.; Theopold, K. H. Binding and Activation of Small Molecules by Three-Coordinate Cr(I). *J. Am. Chem. Soc.* **2007**, *129*, 8090–8091.
- (6) King, E. R.; Hennessy, E. T.; Betley, T. A. Catalytic C–H Bond Amination from High-Spin Iron Imido Complexes. *J. Am. Chem. Soc.* **2011**, *133*, 4917–4923.
- (7) Gehring, H.; Metzinger, R.; Braun, B.; Herwig, C.; Harder, S.; Ray, K.; Limberg, C. An iron(ii) hydride complex of a ligand with two adjacent [small beta]-diketiminato binding sites and its reactivity. *Dalton Trans.* **2016**, *45*, 2989–2996.
- (8) Yu, Y.; et al. The Reactivity Patterns of Low-Coordinate Iron–Hydride Complexes. *J. Am. Chem. Soc.* **2008**, *130*, 6624–6638.
- (9) Smith, J. M.; Lachicotte, R. J.; Holland, P. L. NN Bond Cleavage by a Low-Coordinate Iron(II) Hydride Complex. *J. Am. Chem. Soc.* **2003**, *125*, 15752–15753.
- (10) Holland, P. L. Electronic Structure and Reactivity of Three-Coordinate Iron Complexes. *Acc. Chem. Res.* **2008**, *41*, 905–914.
- (11) Eckert, N. A.; Smith, J. M.; Lachicotte, R. J.; Holland, P. L. Low-Coordinate Iron(II) Amido Complexes of β -Diketiminates: Synthesis, Structure, and Reactivity. *Inorg. Chem.* **2004**, *43*, 3306–3321.
- (12) Lemal, D. M. Perspective on Fluorocarbon Chemistry. *J. Org. Chem.* **2004**, *69*, 1–11.
- (13) Müller, K.; Faeh, C.; Diederich, F. Fluorine in Pharmaceuticals: Looking Beyond Intuition. *Science* **2007**, *317*, 1881–1886.
- (14) Key, B. D.; Howell, R. D.; Criddle, C. S. Fluorinated Organics in the Biosphere. *Environ. Sci. Technol.* **1997**, *31*, 2445–2454.
- (15) Aizenberg, M.; Milstein, D. Catalytic Activation of Carbon–Fluorine Bonds by a Soluble Transition Metal Complex. *Science* **1994**, *265*, 359–361.
- (16) Fischer, P.; Götz, K.; Eichhorn, A.; Radius, U. Decisive Steps of the Hydrodefluorination of Fluoroaromatics using [Ni(NHC)₂]. *Organometallics* **2012**, *31*, 1374–1383.
- (17) Wu, J.; Cao, S. Nickel-Catalyzed Hydrodefluorination of Fluoroarenes and Trifluorotoluenes with Superhydride (Lithium Triethylborohydride). *ChemCatChem* **2011**, *3*, 1582–1586.
- (18) Lv, H.; Zhan, J.-H.; Cai, Y.-B.; Yu, Y.; Wang, B.; Zhang, J.-L. π – π Interaction Assisted Hydrodefluorination of Perfluoroarenes by Gold Hydride: A Case of Synergistic Effect on C–F Bond Activation. *J. Am. Chem. Soc.* **2012**, *134*, 16216–16227.
- (19) Zhan, J.-H.; Lv, H.; Yu, Y.; Zhang, J.-L. Catalytic C–F Bond Activation of Perfluoroarenes by Tricoordinated Gold(I) Complexes. *Adv. Synth. Catal.* **2012**, *354*, 1529–1541.
- (20) Matsunami, A.; Kuwata, S.; Kayaki, Y. Hydrodefluorination of Fluoroarenes Using Hydrogen Transfer Catalysts with a Bifunctional Iridium/NH Moiety. *ACS Catal.* **2016**, *6*, 5181–5185.
- (21) Mai, V. H.; Nikonov, G. I. Hydrodefluorination of Fluoroaromatics by Isopropyl Alcohol Catalyzed by a Ruthenium NHC Complex. An Unusual Role of the Carbene Ligand. *ACS Catal.* **2016**, *6*, 7956–7961.
- (22) Sabater, S.; Mata, J. A.; Peris, E. Hydrodefluorination of carbon–fluorine bonds by the synergistic action of a ruthenium–palladium catalyst. *Nat. Commun.* **2013**, *4*, 2553.10.1038/ncomms3553
- (23) Vela, J.; Smith, J. M.; Yu, Y.; Ketterer, N. A.; Flaschenriem, C. J.; Lachicotte, R. J.; Holland, P. L. Synthesis and Reactivity of Low-Coordinate Iron(II) Fluoride Complexes and Their Use in the Catalytic Hydrodefluorination of Fluorocarbons. *J. Am. Chem. Soc.* **2005**, *127*, 7857–7870.
- (24) Hein, N. M.; Suzuki, T.; Ogawa, T.; Fryzuk, M. D. Low coordinate iron derivatives stabilized by a [small beta]-diketiminato mimic. Synthesis and coordination chemistry of enamidophosphinimine scaffolds to generate diiron dinitrogen complexes. *Dalton Trans.* **2016**, *45*, 14697–14708.
- (25) Dugan, T. R.; Holland, P. L. New routes to low-coordinate iron hydride complexes: The binuclear oxidative addition of H₂. *J. Organomet. Chem.* **2009**, *694*, 2825–2830.
- (26) Yu, Y.; Brennessel, W. W.; Holland, P. L. Borane B–C Bond Cleavage by a Low-Coordinate Iron Hydride Complex and N–N Bond Cleavage by the Hydridoborate Product. *Organometallics* **2007**, *26*, 3217–3226.
- (27) Reger, D. L.; Pascui, A. E.; Smith, M. D.; Jezierska, J.; Ozarowski, A. Halide and Hydroxide Linearly Bridged Bimetallic Copper(II) Complexes: Trends in Strong Antiferromagnetic Superexchange Interactions. *Inorg. Chem.* **2012**, *51*, 7966–7968.
- (28) Frisch, M. J.; et al. *Gaussian 09*; Gaussian Inc: Wallingford, CT, 2009.
- (29) McLean, A. D.; Chandler, G. S. Contracted Gaussian basis sets for molecular calculations. I. Second row atoms, Z = 11–18. *J. Chem. Phys.* **1980**, *72*, 5639–5648.
- (30) Krishnan, R.; Binkley, J. S.; Seeger, R.; Pople, J. A. Self-consistent molecular orbital methods. XX. A basis set for correlated wave functions. *J. Chem. Phys.* **1980**, *72*, 650–654.
- (31) Wachters, A. J. H. Gaussian Basis Set for Molecular Wavefunctions Containing Third-Row Atoms. *J. Chem. Phys.* **1970**, *52*, 1033–1036.
- (32) Hay, P. J. Gaussian basis sets for molecular calculations. The representation of 3d orbitals in transition-metal atoms. *J. Chem. Phys.* **1977**, *66*, 4377–4384.
- (33) Raghavachari, K.; Trucks, G. W. Highly correlated systems. Excitation energies of first row transition metals Sc–Cu. *J. Chem. Phys.* **1989**, *91*, 1062–1065.
- (34) Becke, A. D. Density-functional thermochemistry. III. The role of exact exchange. *J. Chem. Phys.* **1993**, *98*, 5648–5652.
- (35) Lee, C.; Yang, W.; Parr, R. G. Development of the Colle–Salvetti correlation-energy formula into a functional of the electron density. *Phys. Rev. B: Condens. Matter Mater. Phys.* **1988**, *37*, 785–789.
- (36) Vosko, S. H.; Wilk, L.; Nusair, M. Accurate spin-dependent electron liquid correlation energies for local spin density calculations: a critical analysis. *Can. J. Phys.* **1980**, *58*, 1200–1211.
- (37) Stephens, P. J.; Devlin, F. J.; Chabalowski, C. F.; Frisch, M. J. Ab Initio Calculation of Vibrational Absorption and Circular Dichroism Spectra Using Density Functional Force Fields. *J. Phys. Chem.* **1994**, *98*, 11623–11627.
- (38) SAINT, Version 7.03A; Bruker AXS Inc: Madison, WI, 2003.
- (39) SADABS, V2.10; Bruker AXS Inc: Madison, WI, 2003.
- (40) Dolomanov, O. V.; Bourhis, L. J.; Gildea, R. J.; Howard, J. A. K.; Puschmann, H. OLEX2: a complete structure solution, refinement and analysis program. *J. Appl. Crystallogr.* **2009**, *42*, 339–341.
- (41) Sheldrick, G. A short history of SHELX. *Acta Crystallogr., Sect. A: Found. Crystallogr.* **2008**, *64*, 112–122.
- (42) Farrugia, L. J. ORTEP-3 for Windows - a version of ORTEP-III with a Graphical User Interface (GUI). *J. Appl. Crystallogr.* **1997**, *30*, 565–565.